Characterization of defect microstructure in MgRE (RE=Ce, Nd) alloys after processing by High-Pressure Torsion using Positron Annihilation Spectroscopy and a High Resolution X-ray Diffraction

I. Bibimoune[a*], Y. I. Bourezg[a], K. Abib[a], M. O. Liedke[b], A. Wagner[b], Z. Matej[c], Y. Huang[d,e], T. G. Langdon[e], D. Bradai[a]

[a] Faculty of Physics, University of Sciences and Technology Houari Boumediene, Algiers, Algeria.

[b] Institute of Radiation Physics, Helmholtz-Zentrum Dresden – Rossendorf, Bautzner Landstr. 400, 01328 Dresden, Germany

[c] MAX IV Laboratory, Lund University, Fotongatan 2, Lund, Sweden

[d] Department of Design and Engineering, Faculty of Science and Technology, Bournemouth University, Poole, Dorset BH12 5BB, UK

[e] Materials Research Group, Department of Mechanical Engineering, University of Southampton, Southampton SO17 1BJ, UK

[*]Corresponding author: imenebibmoune2017@gmail.com

Abstract

Two MgRE (RE=Ce, Nd) alloys with ultrafine-grain (UFG) microstructures were prepared by high-pressure torsion (HPT) at room temperature. The in-depth distribution of defects was characterized by Doppler broadening –variable energy positron annihilation spectroscopy (DB-VEPAS). The characteristic S parameter increases in bulk after HPT processing relative to an as-received sample and shows a relative stability between ½ and 10 turns, which suggests a rise in the open volume defect density. However, a theoretical analysis of the S(E) depth profile reveals an increase in the positron diffusion length from ~115 nm for the as-received state to

~207 nm after 10 HPT turns. Almost all the open volume defect consisted of dislocations (positron lifetime of τ = 260 ps). The dislocation density deduced from high-resolution X-ray diffraction in the HPT disc radial direction was reasonably homogeneous (around 4-6 $\times 10^{14}$ m^{-2}).

Keywords : Mg; rare earth; HPT; Dislocations; Positron; Spectroscopy.

1 Introduction

Magnesium alloy sheets have motivated many research activities owing to their potential applications as structural parts in the automotive industry due to the exceptional low density and high specific strength of magnesium. Nevertheless, magnesium sheets usually suffer from a poor ductility and strong anisotropy at ambient room temperature [1] and this limits their forming and hence their industrial applications [2]. In order to improve the ductility and lower the anisotropy by the control of the crystallographic texture, many non-conventional or severe plastic deformation (SPD) techniques, such as equal-channel angular pressing (ECAP) [3], differential speed rolling [4], torsion extrusion [5] and high-pressure torsion (HPT) [6], have been applied to magnesium alloys and this has proven effective in developing weaker or non-basal textures. Besides the application of non-conventional deformation techniques, RE additions like Ce and Nd were found to randomize the texture and alter recrystallization processes [7]. Indeed, individual RE elements have been used as alloying additions for more than three decades [8].

Among the various SPD techniques, HPT is known to introduce a high density of lattice defects that are responsible for exceptional mechanical and physical properties of ultrafine-grained (UFG) materials. Consequently, a determination of the nature and amount of these defects is essential.

Positron annihilation spectroscopy (PAS) has been considered a powerful and promising direct and non-destructive method showing a high sensitivity to open-volume defects such as vacancies, vacancy clusters and dislocations [9, 10]. In order to achieve a deeper insight, PAS is often coupled with scanning electron microscopy-electron backscatter diffraction (SEM-EBSD) and transmission electron microscopy (TEM) for metallography, X-ray diffraction line profile analysis (XRDLPA) for microstructure and microhardness for the mechanical properties.

The PAS techniques has a great potential when it probes light alloys which undergo age-hardening, grain refinement, fatigue and fracture owing to the direct impact of the technology [11].

A non-exhaustive review of the literature shows that Mg in general and Mg-RE alloys were the subjects of much research dealing with post-deformation defects analysis. The principal results so far were conducted on Mg, Mg-Gd and Mg-Tb-Nd alloys primarily processed by HPT [12-14]. There is no doubt that Mg alloyed with Ce and Nd has motivated very significant interest over the last few years.

Accordingly, in the present work two different PAS techniques were used. Firstly, Doppler broadening – variable energy PAS (DB-VEPAS [15]) for the identification of the in-depth distribution of defects, and secondly PA-lifetime spectroscopy (PALS) for the identification of the defect nature and density in bulk. Additionally, high-resolution X-ray diffraction measurements were carried out in order to determine the dislocation density in the radial direction of the HPT-processed discs.

2 Experimental materials and procedures

Full details of the Mg-Re (RE=Ce, Nd) alloys and their severe plastic deformation by HPT are available in earlier reports [16-17].

The PAS measurements were conducted at the Institute of Radiation Physics at Helmholtz-Zentrum Dresden Rossendorf (HZDR). The SPONSOR (Slow POsitroN System Of Rossendorf) at HZDR [15] and a conventional lifetime spectrometer were used. Positron energies E from the SPONSOR beam varied between 0.03 and 35 keV.

The results were analyzed using the versatile software package VEPFIT [18]. The S(E) plot was then fitted and the positron energies were converted into a depth scale. The VEPFIT program (VF2021) solves the full positron implantation-diffusion problem for any layered system with proper thickness and diffusion length [19].

DB-VEPAS utilizes a high purity Ge-detector with a resolution $f_R = 1.09 \pm 0.01$ keV at 511 keV. Implanted into samples, positrons lose their kinetic energy due to thermalization and after short diffusion they are annihilated in delocalized lattice sites or they become localized in vacancy-like defects and interfaces emitting usually two anti-collinear 511keV gamma photons once they meet electrons. At the annihilation site, the thermalized positrons have very small momentum compared to the electrons and therefore a broadening of the 511 keV line is observed mostly due to the momentum of the electrons. The broadening of the annihilation spectrum is characterized mainly by the so-called S-parameter, which is a fraction of the annihilation line in the middle (511±0.74 keV) of the spectrum. If a sample contains many defects in the near surface, more positrons would annihilate in these defects than in the bulk leading to a higher S parameter. However, a different phase owns a different characteristic S-parameter, and thus it is possible to predict the defect nano-structure in the sub-surface region of the samples. The S-parameter is the fraction of positrons annihilating with low momentum valence electrons and it represents vacancy-type defects and their concentration detected across the sample thickness down to some micrometers [15]. The w-parameter was also considered and is associated with the high momentum core electrons which is more sensitive to the chemical surrounding of the annihilation sites.

Contrary to DB-VEPAS, the conventional positron lifetime (PL) technique provides information on the volume properties of the specimens.

A PL spectrometer with a time resolution of 230 ps (full-width at half maximum (FWHM) of the resolution function) and a positron source with a 22Na radioisotope covered with a 2μm thick Al foil was used and was described in detail in another report [20]. A minimum of 10^6 counts was necessary in order to analyze the measured spectra. LT10 software [21] was used for the decomposition of the PALS spectra into exponential components using a two states trapping model, and a Si reference sample with a single lifetime of 218 ps was used for the evaluation of the source contribution which was around 21%. The source contribution consisted of three components with lifetimes of 380 ps from positrons annihilated in the 22Na source, 165 ps from positrons annihilated in the covering Al foils and 1140 ps for surface effects. This long component was always present and remained almost constant as already mentioned in another report [22].

The X-ray diffraction experiments were conducted at the beam-line I711 of Max-II [23] (MAX IV Laboratory in Lund, Sweden). Wide range high resolution X-ray diffraction patterns were recorder by a Pilatus 100K hybrid photon counting area detector. The detector was mounted on the long goniometer arm and a wide angular range was scanned by continuously moving the detector and integrating diffracted X-ray intensity [24]. All experiments were conducted at the room temperature. Samples were measured in the reflection geometry with a constant incidence angle of the X-ray beam irradiating a limited sample area. The X-ray wavelength was equal to 0.9938 Å.

The computer program MStruct [25] was used for the fitting of the measured XRD patterns. Using this software it was possible to reveal the phase composition and the details of the real

structure of the investigated material, such as the lattice parameters, the size of coherently diffracting domains, the dislocation density and the micro-strain [14].

3 Results and Discussion

3.1 Near surface defect analysis

Figure 1 shows the S(E) parameter as a function of the incident positron energy in the as-received MgRE (RE=Ce, Nd) (N=0) and in MgNd samples after HPT deformation through N=1/2 and 10 where N is the number of HPT turns.

The S-parameter increases in bulk after deformation, which is explained by the increase in defect density and trapping sites in the material. In practice, with respect to a defect-free reference sample (the as-received sample in the present study), more annihilation of positrons in vacancies produces a narrowing of the annihilation peak and therefore an increase of S(E).

The S(E) parameters of the as-received MgCe and MgNd and HPT processed MgNd alloys up to ½ and 10 turns exhibit almost the same evolution. Apart from the fact that the S(E) of the as-received MgCe alloy shows a larger than saturation value of the S(E) for 1 keV< E <15 keV. This is indicative of the presence of a surface oxide film, which contains many open volume defects which are probably voids [26].

The quasi-stabilization of S(E) between ½ and 10 turns means that the defect density saturated shortly after ½ turn. The curve of S as a function of the implantation energy reaches saturation from an energy equal to 15 KeV, which is equivalent to an implantation depth of 1.66 µm. From 1.66 µm the defect density in the material becomes homogeneous. The implantation depth was calculated using an equation assuming a Makhovian profile [19]:

$$z = \frac{3.6E^n}{\rho} \quad (1)$$

where E is the implantation energy in keV, the n parameter was set equal to n =1.62 and the density of the Mg was $\rho = 1.74$ g/cm^3.

The VEPFIT software [18] was used in order to determine the thickness of the sub-surface layer d as well as the diffusion lengths of positrons in the sub-surface layer L_{1+} and bulk L_{2+} and the results are presented in Table 1. The diffusion length, corresponding to the average distance L that positrons in thermal equilibrium with the environment can travel before being annihilated, was determined using the VEPFIT package [18]. The value of the bulk positron diffusion length determined in MgCe and MgNd before deformation was 46±13 and 115±25 nm, respectively, which is lower than the tabulated value in the literature for bulk magnesium (192-200 nm) [19, 26] and hence represents a probable defect state. These values are lower compare with an estimated positron diffusion length for defect-free Mg of $L_+ = \sqrt{D_+ \tau} \cong 192\ nm$ at ambient temperature. This last value was assessed using $\tau = 210$ ps in bulk Mg and $D_+ = 1.67$ cm^{2}s^{-1} calculated using an *ab initio* method [27-29]. In addition, both as-received samples exhibit thin sub-surface layers of ~16 and ~ 44 nm, respectively, where L_+ is below 16 nm and probably consists of oxides.

The positron diffusion length in undeformed Mg-Ce and Mg-Nd alloys is ~ 4 times and ~2 times, respectively, smaller than the values reported for annealed bulk Mg. This suggests that these alloys contain a certain density of defects, which could be considered as low.

After deformation, the positron diffusion length in the bulk increases so that L_{2+}=146±71 nm for ½ turn and L_{2+}=207±68 nm for 10 turns HPT. The increase of L+ indicates a substantial reduction of defect density including a complete disappearance for the latter. On the other hand, the L_+ in the sub-surface layer raises for ½ turn to L_{1+}~48 nm and then drops to only L_{1+}~8 nm for 10 turns. Moreover, the thickness of the sub-surface layer increases to d~162 and ~129 nm. The defect density of the sub-surface layer is larger than estimated for the bulk and its depth is

probably not larger than 200 nm. Unfortunately, there are no available diffusion length data in Mg-based alloys either conventionally processed or after severe plastic deformation. In pure copper severely deformed by ECAP and HPT, there were diffusion lengths of 42 and 35 nm [30], respectively. These trends are much different to the present results and they are closer to the diffusion length in undeformed pure copper, ~146 nm [31]. The drastic decrease of the diffusion length in the severely deformed materials is a direct consequence of the large defect density and trapping centers. The present findings suggest the opposite trend with a reduction of defect concentration, at least in the first 6-10 μm, or alternatively a reduction of positively charged defects such as monovacancies.

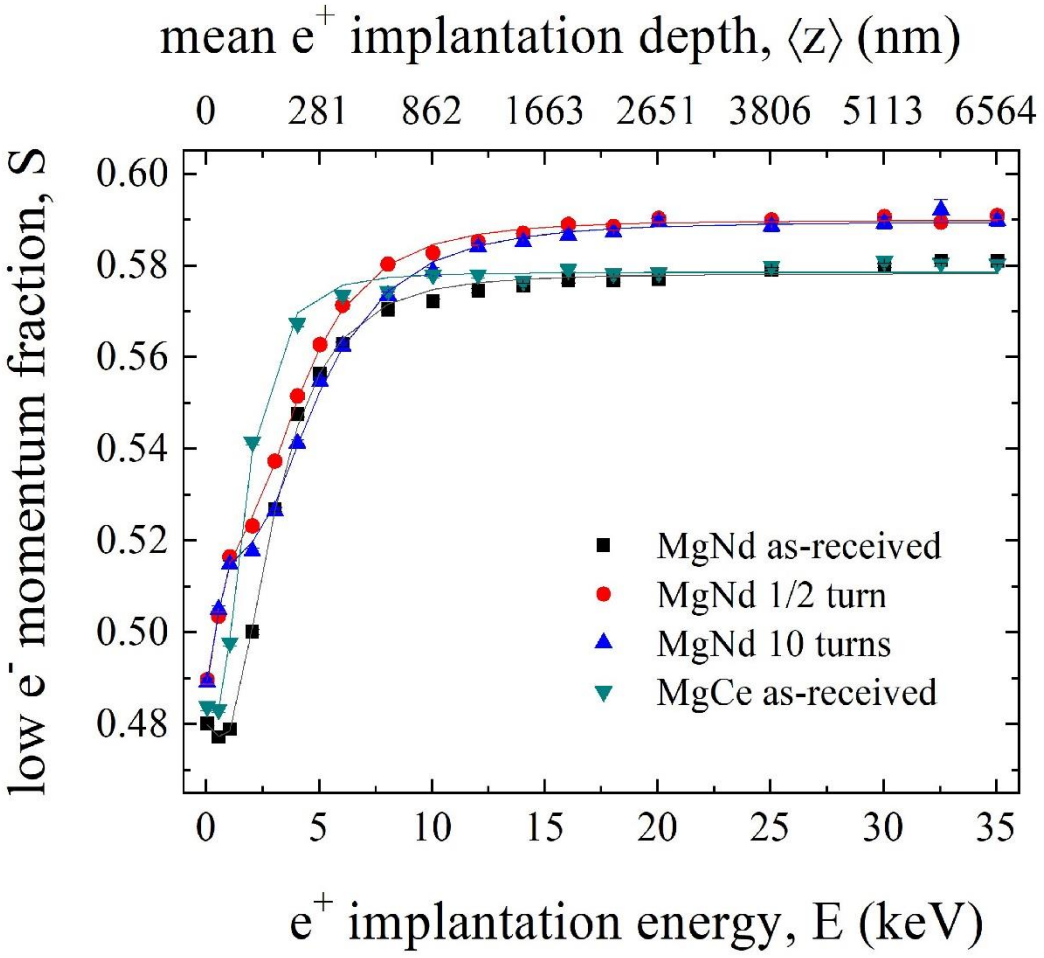

Figure 1 S(E) parameter plot data with fitted dependence in MgRE (RE=Ce, Nd) alloy after HPT processing.

Table 1 Calculated thickness of the sub-surface layer d, positron diffusion lengths in the sub-surface layer L_{1+} and bulk L_{2+} in MgRE (RE=Ce, Nd) alloy after HPT processing. The values without errors were fitted as fixed accounting for the lowest chi-square. All length values are in nm.

MgCe N=0			MgNd N=0			MgNd N=1/2			MgNd N=10		
d	L_{+1}	L_{+2}	d	L_{+1}	L_{+2}	d	L_{+1}	L_{+2}	d	L_{+1}	L_{+2}
16±14	2	46±13	44	16	115±25	162	48	146±71	129±42	8±3	207±68

3.2 Bulk defects analysis; positron lifetime spectroscopy

Figure 2 a and b present the results of positron lifetime evolution and relative intensity, respectively, versus the HPT number of turns in MgCe and MgNd alloys. In the measured spectra, two lifetime components were resolved. The first component (185-220 ps) corresponds to the lifetime value of positrons annihilated in bulk, which is in good agreement with the tabulated values [32] for three AE21, AE42 and LAE442 magnesium alloys after ECAP processing.

Clearly the lifetime of this component decreases abruptly from the undeformed sample to the N=0.5 HPT processed sample. Such a decrease has also reported earlier [32] but without any explanation. The lifetime seems to stabilize between N=0.5 and N=5 and experiences a faint second drop. This decrease may be associated with the lattice parameter distortion due to the intense stress during HPT processing. Indeed, HPT processing among severe plastic deformation techniques is the one that introduces the more intense amount of dislocations. Phenomenologically, it is expected that with the reduction of the unit cell volume, the electronic density should increase and hence the lifetime of free positions should decrease. However, this is not the case for Mg-based alloys since processing by HPT leads to an increase of the unit cell

volume [33] and therefore this effect was not effective in the reduction of the bulk positron lifetime. The intensity of the second component associated with dislocations supports this assumption since it gains +70% above N=0.5 turns so that the dislocations constitute the dominant trapping-annihilation sites. The second drop after N=5 turns is probably associated with dynamic recovery.

In earlier work a solution treated Mg22Gd sample exhibited a single component LT spectrum with lifetime of (226 ps) [14] while there were two components in a homogenized Mg10Gd alloy [12]. It was assumed that there was an absence of defects component in the Mg22Gd alloy and/or their density was very low so that virtually all positrons were annihilated in the free state and not trapped at defects. An alternative explanation was that the low dislocation density in the specimen approached the lower sensitivity limit of PL spectroscopy [12]. Therefore, positrons trapped at dislocations cannot provide a significant contribution to the PL spectrum [12].

The present results show that, unlike the Mg-22Gd alloy (I_D < 25 %), non-negligible amounts (I_D = 54-63 %) of dislocations remain after solution annealing of the Mg-RE (RE=Ce, Nd). This discrepancy may be explained by the fundamental chemical difference between the studied alloys. Indeed, Mg22Gd alloy contain many more solute atoms than Mg1.43Ce and Mg1.42Nd and this should considerably modify the defects annihilation. It is worth noting also that the solution annealing of the Mg-22Gd alloy led to a hardness almost twice that of the Mg1.43Ce and Mg1.42Nd alloys [34]. The process of homogenization and defects (dislocations and vacancies) release during the solution annealing may be different with respect to the chemical species and their concentration. However, the interplay between the solute nature and the defect density is not yet understood and more research is needed.

The second component (257-262 ps) corresponds well with tabulated values in the literature for positrons trapped and annihilated at dislocations. Table 2 summarizes an updated published lifetime of the components in Mg-based alloys.

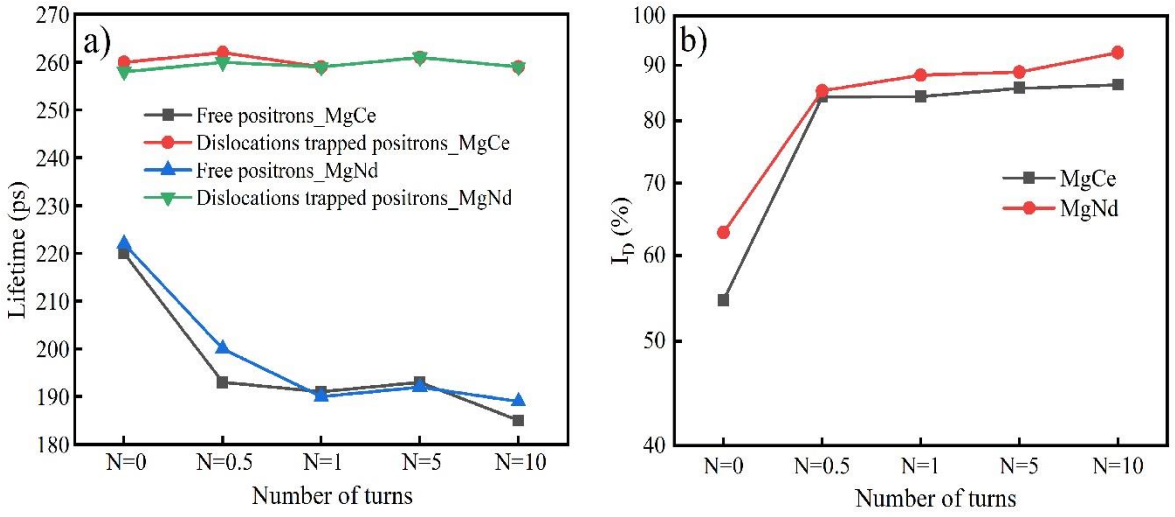

Figure 2 Results of lifetime investigations of HPT deformed MgCe and MgNd alloys, (a) variation of the lifetime of the positrons annihilated in the bulk and trapped in the dislocations, (b) variation of intensity of trapped dislocation, as a function of the number of HPT turns.

Table 2 Positron lifetimes in free state (τ_{Free}) and defect-trapped state in dislocation (τ_D) in pure Mg and Mg alloys processed by SPD technique according to published data.

Alloy	Experimental conditions	Major results	Ref
Mg	HPT	τ_{Free}= 188 ps, τ_{D}= 257 ps	J. Čížek /2007
Mg10Gd	P = 5GPs	τ_{Free}=180 ps, τ_{D}= 256 ps	[12]
	N = 5 turns		
Mg-22%wtGd	HPT	τ_{Free}= 210-227 ps, τ_{D}= 250 ps	J. Čížek/2017
	P = 2GPs		[14]
	N = 1/4, 1/2, 1, 2, 3, 5, 10, 15 turns.		
Mg-3Tb-2Nd	HPT	τ_{Free} = 90-230 ps, τ_{D}= 256 ps	J. Čížek /2009
Mg-9-Gd	P = 6GPs	τ_{Free} = 180-224 ps, τ_{D}= 256 ps	[13]
	N = 5 turns		
AE21	ECAP (route Bc)	τ_{Free} = 198-216 ps, τ_{D} = 255 ps	P. Minarik/2016
AE42	N = 1-12 passes	τ_{Free} = 220-222 ps, τ_{D} = 255 ps	[32]
LAE442		τ_{Free} = 150-200 ps, τ_{D} = 255 ps	
MgCe	HPT	τ_{Free} = 185-220 ps, τ_{D} = 260 ps	present results
MgNd	P = 6GPs	τ_{Free} = 189-222 ps, τ_{D} = 260 ps	
	N = 5 turns		

Dislocation lines represent only weak traps for positrons unlike the point defects associated with dislocations that could represent more efficient trapping sites [22]. The lifetime associated with deformation-induced dislocations in a Mg monocrystal was about 249 ps while that corresponding to monovacancies was 255 ps. Therefore, these values are very close and within statistical scatter.

It is assumed that positron trapping at dislocations is a two-stage process [35]. Shallow traps in the dislocation core act as first positron trap centers. There will be a subsequent rapid diffusion of these localized positrons along the dislocation line and eventually a second trap will operate. These secondary traps are vacancies anchored in the elastic field of the dislocation [35, 36]. Furthermore, it has been well established that in Mg the positron trapping rate in defects is relatively low [37, 38] and the trapping sites are shallow [39].

Recently, it was shown that positron lifetimes (τ=254 ps) in extruded Mg–0.45wt%Zn–0.45wt%Ca (ZX00) is close to those of dislocations (τ=256 ps) and smaller than those of vacancies (τ=297 ps) [40]. These lifetimes were attributed to the trapping and annihilation in grain boundaries and matrix–precipitate interfaces. The grain boundaries are considered as extended defects and they are the major type of positron trap where this assumption was validated by a diffusion-reaction model for positron trapping and annihilation in a fine-grained structure.

Positrons may also be trapped by grain boundaries provided that the overall grain size is smaller than the positron diffusion length. This may not be the case in the present study since the grain size of Mg-based alloys never reaches such low values even after the most severe plastic deformation by HPT [16] owing to the occurrence of dynamic recrystallization. Moreover, grain boundaries are disordered regions containing open-volume sites and thus must be considered as potential positron traps. The possibility of localizing a substantial fraction of

positron annihilations inside the grain boundary region suggests the application of various PAS techniques to study local morphological and chemical characteristics [11].

Undoubtedly, the nodal parameter of the problem is the ratio between the linear size of the grain R and the positron diffusion length (L_+). As seen above, the positron diffusion length is $L_+ \approx$ 192 nm in non-deformed MgRE alloys while the grain size is far greater. Consequently, any consideration of the grain boundaries as major players while using PAS becomes marginal in fine-grained alloys, but this consideration should be possible for nano-sized alloys [11].

Such values have been attributed to the positron lifetime trapped at single vacancies [41]. It was also suggested that in the case of magnesium the obtained positron lifetime is an averaged value over different states where positrons can be trapped mainly at the dislocation jogs which are formed by dislocation intersections.

Positron annihilation spectroscopy was used to determine the lifetimes of annihilated positrons in Mg-based alloys (AE21, AE42 and LAE442 alloys) after ECAP processing up to 12 passes using processing route Bc and this revealed two components [32]. The first component corresponded to the annihilation of positrons in the bulk with a value is between 150 and 220 ps. The second component with a value of 255 ps, was assigned to positrons trapped at dislocations introduced during plastic deformation.

Figure 2b shows the variation of intensity of trapped dislocations as a function of the number of HPT turns. The intensity for the MgCe alloy increases from 54% to 84% and for MgNd from 63% to 85% after a half turn of HPT which corresponds to an equivalent strain close to nine, and afterwards there is a very small increase for both alloys which means that a saturation of the microstructure takes place at the initial stage of the deformation. The high value of I_D means that almost all positrons are trapped in dislocations and a few positrons are annihilated in the bulk. It is interesting to note that a similar microhardness evolution was reported in an earlier

study of MgRE (RE=Ce, Nd) under the same deformation conditions [16], which shows that the microhardness increases significantly after N=1/2 turn and reaches saturation after N=1 HPT turn.

The development of the microstructure during HPT treatment of Mg22Gd was studied using a combination of PAS and X-ray line profile analysis (XLPA) [14]. Analyses of their spectra showed two lifetime components, τ_1 =225-210 ps and τ_2=250 ps with intensity between 25 and 55%.

Figure 3 shows the evolution of the dislocation density as a function of the applied strain. The equivalent strain ε_{eq} is calculated using the following equation [42].

$$\varepsilon_{eq} = \frac{2\pi r N}{t\sqrt{3}} \qquad (2)$$

where r, t and N are the radial distance from the center of the disk, the thickness of the deformed sample and the HPT turn number, respectively.

The dislocation density in the deformed alloys was calculated from the PALS versus the τ_1 and τ_2 parameters using the two state simple trapping model (STM) [32].

$$\rho = \frac{1}{\nu} I_2 \left(\frac{1}{\tau_1} - \frac{1}{\tau_2}\right) \qquad (3)$$

where ν is the specific positron trapping rate for dislocations in Mg and its alloys ($\nu = 10^{-5}$ m^{-2} s^{-1} [32].

The use of equation (3) is valid since in Mg-RE alloys the spatial distribution of dislocations is uniform and the assumptions of the Simple Trapping Model are usually fulfilled [43]. Indeed, evidence was presented of a microstructure consisting of dense forest of dislocations blocking each other where the dislocation lines are split to partial dislocations in Mg-10 wt%Gd alloy deformed by HPT [12].

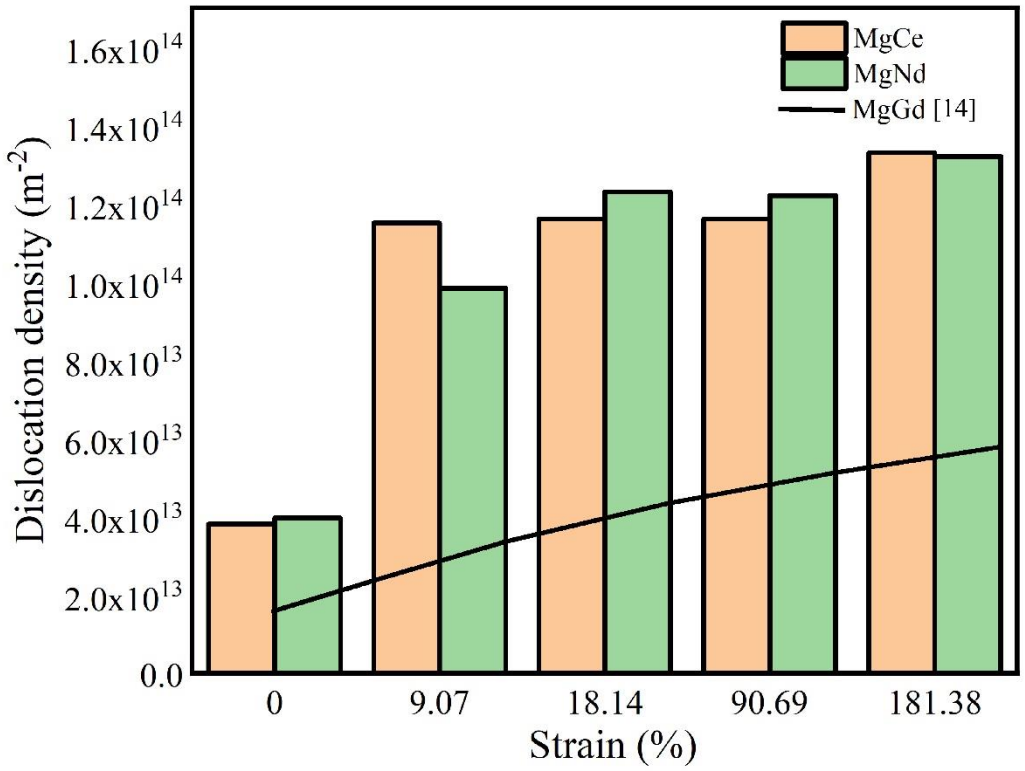

Figure 3 Evolution of the dislocation density as a function of the applied strain calculated from PALS parameters. The data extracted from reference [14] associated with Mg-22Gd alloys are given for comparison.

The histogram in Figure 3 demonstrates the dislocation density evolution in Mg1.43Nd and Mg-1.44Ce HPT-processed discs up to 10 turns.

The dislocation density calculated by PALS using equation (3) near the edge of the different HPT processed Mg-RE (Ce, Nd) samples, (N=0, N=1/2, N=1, N=5, N=10 turns) shows a rapid increase after the application of an equivalent strain equal to 9 (N=1/2), while there is evidence for a very slight evolution afterwards. The dislocation density of the as-received alloys is rather weak (3. 9× 10^{13} m^{-2}). Its evolution is almost similar and then reaches a saturation near 1.33 ×10^{14} m^{-2} for both alloys.

A fast comparison with the data tabulated elsewhere [14] suggests a qualitative agreement with the present results. However, the present dislocation values are about twice to three time greater than those for the Mg22Gd alloy. The dislocation density was evaluated from the mean of the calculated values near the center, the middle and edge of the discs [14] and there was evidence for a uniform distribution of dislocations in HPT-deformed Mg22Gd alloy via TEM observations. Such a microstructure is often observed in hcp metals subjected to severe plastic deformation and it is a consequence of the lack of sufficient active slip systems in the hcp structure so that the dislocations block each other and tangles of dislocations are formed [14]. The severe plastic deformation microstructure developed in the FCC and BCC structure is rather different and is of a cellular dislocation structure [44, 45].

3.3 Bulk defect analysis; high resolution X-ray diffraction

Figure 4 shows the XRD patterns of the HPT-processed MgNd and MgCe alloys up to 10 turns at the location near the center of the disc (r=R/2). The patterns of the remaining samples are not shown because of their similarity. Inspection of these patterns shows that the use of a monochromatized synchrotron beam easily reveals the different precipitate peaks that are often obscured in the background when using more conventional XRD techniques.

In addition to the existence of the hcp α-Mg matrix phase, some precipitates are easily indexed. As is apparent from inspection of Figure 4, the XRD patterns of the HPT-processed alloys show that the Mg-1.44Ce alloy has a certain volume fraction, proportional to their intensities, of two second phases identified as $MgCe_2$ (space group I4/mmm, a = b= 1.036 nm and c = 0.596 nm) and $Mg_{17}Ce_2$ (space group P63/mmc, a = b= 1.035 nm and c = 1.026 nm).

By contrast, smaller amounts of the $Mg_{12}Nd$ phase (space group I4/mmm, a = b = 1.031 nm and c = 0.593 nm) exist in the Mg-1.43Nd alloy. The volume fraction of precipitates determined from a quantitative analysis using MAUD software [46] were as follows: Fv ($Mg_{17}Ce2$) = 4–4.5 % and Fv ($Mg_{12}Nd$) = 1–1.5 % and obviously there was no variation upon straining. The

existence of these precipitates is due to their incomplete dissolution during the solution annealing at 535 °C for 5 h [16].

The mean lattice parameters of the matrix α-Mg phase are slightly higher (0.3214 and 0.5215 nm) than those of pure Mg (0.3209 and 0.5211 nm) due to dissolved Ce and Nd atoms. The lattice expansion with respect to pure Mg is 0.83% and 0.12% for the a and c axis, respectively. The dislocation density was calculated using the MStruct software [25] which is a free computer program based on Rietveld refinement and whole powder pattern modelling [47, 48] hat are commonly used for microstructure analysis from powder diffraction data.

The two parameters q_1 and q_2 together with $\bar{C}_{hk,0}$ used for the calculation of the average contrast factors $\bar{C}_{hk,l}$ for pure Mg were taken from [49] Among the deformation modes, the basal slip system was considered as dominant [50] then q_1, q_2 and $\bar{C}_{hk,0}$ were 0,194, 0.0678 and -0.197, respectively. One of the first comprehensive accounts of the dislocation contrast factors in hexagonal crystals was given by Kuzel and Klimanek [51, 52]. The contribution of the precipitates to the broadening was not considered.

Figure 5 shows the dislocation density in three different locations of the HPT discs in the radial direction. The representative positions are near the center, at the mid-radius and near the edge of the HPT-processed samples with 1 and 10 turns. A high-resolution synchrotron XRDLPA technique was used and the dislocation density was calculated using the MStruct software.

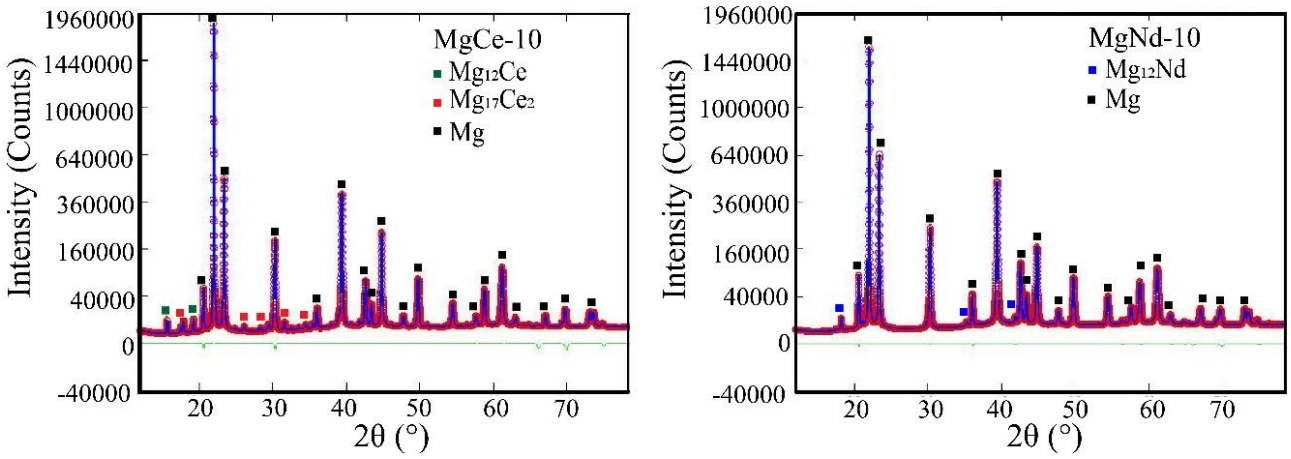

Figure 4 XRD pattern of the HPT processed MgNd and MgCe alloys up to 10 turns at the location near the center of the disc.

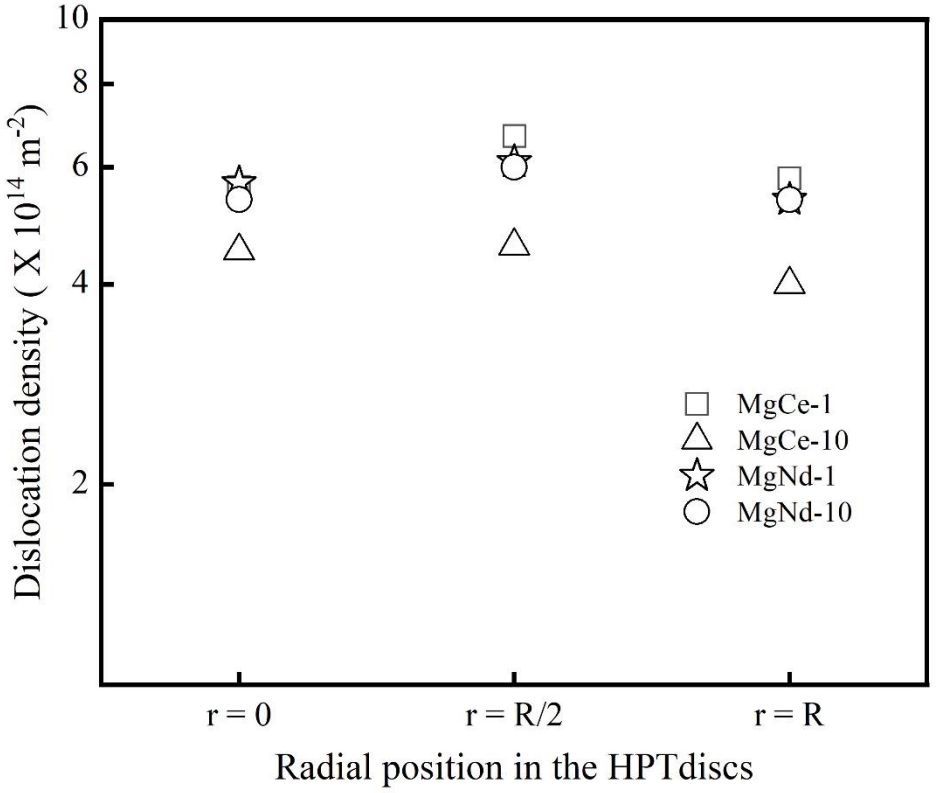

Figure 5 Dislocation density in three different locations of the HPT processed discs in the radial direction calculated using a high-resolution X-ray diffraction.

Interestingly, the dislocation density after HPT processing shows a very faint difference in the radial direction for both alloys. There is a little increase of the dislocation density from r=0 to r=R/2 and then there is an unexpected relative decrease at r = R. Such radial evolution of the dislocation density has never been analyzed so far and many investigations revealed a saturation of the microhardness soon after the first HPT turn [16, 53-55]. Recall that the dislocation density and the microhardness are often well correlated. A uniform distribution of dislocations was reported in the HPT-deformed Mg22Gd alloy using the TEM technique [14] and this suggests that the drop of the dislocation density near the edge of the discs is probable recovery that arises due to the intense strain associated with processing by HPT.

The dislocation density values obtained from the high resolution-synchrotron XRDLPA technique are slightly higher than those estimated from the PALS parameters (Equation 3). The dislocation density was determined using the three techniques of PALS, XRDLPA and SEM [14] and it was found that the value estimated by TEM is in very reasonable agreement with the results of PALS investigations (~10^{14} m^{-2}) but these values were lower than those derived from XRDLPA. It is well known that the broadening of the X-ray diffraction peaks is not only caused by the grain refinement but also by the internal stresses. An additional broadening of the X-ray profile to the modulation of the lattice formed by the different precipitates existing in the matrix was attributed to the limitation of the crystal domains and the inter-domain interactions as well as deformation twins [14]. Furthermore, the rapid saturation of the dislocation density after only one HPT turn is due to the recovery phenomenon that starts at low temperatures (around room temperature) in HPT-deformed Mg alloys [56].

The dislocation density in a Mg-8.2Gd-3.8Y-1.0Zn-0.4Zr alloy (wt.%) after HPT processing up to 16 turns was determined using conventional XRD and, Rietveld refinement [57] and there was evidence of a net saturation around 4.8 ×10^{14} m^{-2} which is reasonably close to the present values determined by MStruct (~ 4.5-6 × 10^{14} m^{-2}).

Summary and conclusions

The defect microstructure in MgRE (RE=Ce, Nd) alloys after processing by High-Pressure Torsion was characterized by Positron Annihilation Spectroscopy and High Resolution X-ray Diffraction. The characteristic S(E) parameter of the Doppler broadening PAS increases after HPT processing relative to an as-received sample (N=0) and shows a relative stability between ½ and 10 turns and this is indicative of open volume defects. A noticeable increase of the positron diffusion length in bulk from ~115 nm (N=0) to 207 nm (N=10) for the Mg-Nd alloy after HPT means that the number of cationic defects has been reduced. This is probably related to a reduction in the number of single vacancies associated with dislocations due to HPT. The dominant type of open volume defect in Mg-RE (RE=Ce, Nd) is identified via lifetime spectroscopy (PALS) as dislocations (τ = 260 ps). Their relatively high intensity confirms that almost all positrons get trapped in the dislocations before they are annihilated. The dislocation density deduced from high-resolution X-ray diffraction is reasonably homogeneous around (4-6 $\times 10^{14}$ m^{-2}) but a certain recovery occurs near the edge of the HPT-processed discs where the applied strain is the highest.

Acknowledgement

The authors are grateful to Dr. W. Anwand (Helmholtz-Zentrum Dresden – Rossendorf, Germany) for performing the DB-VEPAS measurements. One of the authors (DB) thanks Dr. Olivier Balmes (MAX IV Laboratory (Lund, Sweden) for his kind invitation and for the access to I711 beamline.

References

[1] T. Mukai, M. Yamanoi, H. Watanabe, K. Ishikawa, K. Higashi, Effect of Grain Refinement on Tensile Ductility in ZK60 Magnesium Alloy under Dynamic Loading. Mater. Trans. (2001), 42 (7), 1177–1181. https://doi.org/10.2320/matertrans.42.1177.

[2] H. Yan, R.S. Chen, E.H. Han, Room-Temperature Ductility and Anisotropy of Two Rolled Mg–Zn–Gd Alloys. Mater. Sci. Eng. A (2010), 527 (15), 3317–3322. https://doi.org/10.1016/j.msea.2010.02.038.

[3] R.Z. Valiev, T.G. Langdon, Principles of equal-channel angular pressing as a processing tool for grain refinement. Progress in Materials Science. (2006), 51 (7), 881-981. https://doi.org/10.1016/j.pmatsci.2006.02.003

[4] W. Polkowski, Differential Speed Rolling: A New Method for a Fabrication of Metallic Sheets with Enhanced Mechanical Properties. In Progress in Metallic Alloys; Glebovsky, V., Ed.; InTech, 2016. https://doi.org/10.5772/64418.

[5] X. Ma, M.R. Barnett, Y.H. Kim, Forward Extrusion through Steadily Rotating Conical Dies. Part I: Experiments. International Journal of Mechanical Sciences (2004), 46 (3), 449–464. https://doi.org/10.1016/j.ijmecsci.2004.03.017.

[6] A.P. Zhilyaev, T.G. Langdon, Using high-pressure torsion for metal processing: Fundamentals and applications. Progress in Materials Science. (2008), 53 (6), 893-979. https://doi.org/10.1016/j.pmatsci.2008.03.002.

[7] N. Stanford, D. Atwell, A. Beer, C. Davies, M.R. Barnett, Effect of Microalloying with Rare-Earth Elements on the Texture of Extruded Magnesium-Based Alloys. Scr. Mater. (2008), 59 (7), 772–775. https://doi.org/10.1016/j.scriptamat.2008.06.008.

[8] K. Bryła, J. Dutkiewicz, L.L. Rokhlin, L. Litynska-Dobrzynska, K. Mroczka, P. Kurtyka, Microstructure and Mechanical Properties of Mg-2.5%Tb-0.78%Sm Alloy After Ecap and Ageing. Arch. Metall. Mater. (2013), 58 (2), 481–487. https://doi.org/10.2478/amm-2013-0022.

[9] C. Hugenschmidt, Positrons in Surface Physics. Surf. Sci. Rep. (2016), 71 (4), 547–594. https://doi.org/10.1016/j.surfrep.2016.09.002.

[10] J. Čížek, M. Janeček, T. Krajňák, J. Stráská, P. Hruška, J. Gubicza, H.S. Kim, Structural Characterization of Ultrafine-Grained Interstitial-Free Steel Prepared by Severe Plastic Deformation. Acta Mater. (2016), 105, 258–272. https://doi.org/10.1016/j.actamat.2015.12.039.

[11] A. Dupasquier, G. Kögel, A. Somoza, Studies of Light Alloys by Positron Annihilation Techniques. Acta Mater. (2004), 52 (16), 4707–4726. https://doi.org/10.1016/j.actamat.2004.07.004.

[12] J. Čížek, I. Procházka, B. Smola, I. Stulíková, R. Kužel, Z. Matěj, V. Cherkaska, R.K. Islamgaliev, O. Kulyasova, Microstructure and Thermal Stability of Ultra Fine Grained Mg-

Based Alloys Prepared by High-Pressure Torsion. Mater. Sci. Eng. A (2007), 462 (1–2), 121–126. https://doi.org/10.1016/j.msea.2006.01.177.

[13] J. Čížek, I. Procházka, B. Smola, I. Stulíková, M. Vlach, V. Očenášek, O.B. Kulyasova, R.K. Islamgaliev, Precipitation Effects in Ultra-Fine-Grained Mg–RE Alloys. Int. J. Mater. Res. (2009), 100 (6), 780–784. https://doi.org/10.3139/146.110103.

[14] J. Čížek, P. Hruška, T. Vlasák, M. Vlček, M. Janeček, P. Minárik, T. Krajňák, M. Šlapáková, M. Dopita, R. Kužel, T. Kmječ, J.G. Kim, H.-S. Kim, Microstructure Development of Ultra Fine Grained Mg-22 Wt%Gd Alloy Prepared by High Pressure Torsion. Mater. Sci. Eng. A (2017), 704, 181–191. https://doi.org/10.1016/j.msea.2017.07.100.

[15] W. Anwand, G. Brauer, M. Butterling, H.R. Kissener, A. Wagner, Design and Construction of a Slow Positron Beam for Solid and Surface Investigations. Defect Diffus. Forum (2012), 331, 25–40. https://doi.org/10.4028/www.scientific.net/DDF.331.25.

[16] Y.I. Bourezg, H. Azzeddine, T. Baudin, A.-L. Helbert, Y. Huang, D. Bradai, T.G. Langdon, Texture and Microhardness of Mg-Rare Earth (Nd and Ce) Alloys Processed by High-Pressure Torsion. Mater. Sci. Eng. A (2018), 724, 477–485. https://doi.org/10.1016/j.msea.2018.03.114.

[17] Y. I. Bourezg, H. Azzeddine, K. Abib, Y. Huang, D. Bradai, T.G. Langdon, Recrystallization in an Mg-Nd Alloy Processed by High-Pressure Torsion: A Calorimetric Analysis. J. Mater. Res. Technol. (2020), 9 (3), 3047–3054. https://doi.org/10.1016/j.jmrt.2020.01.035.

[18] A. van Veen, H. Schut, M. Clement, J.M.M. de Nijs, A. Kruseman, M.R. IJpma, VEPFIT applied to depth profiling problems, Appl. Surf. Sci. 85 (1995) 216–224. https://doi.org/10.1016/0169-4332(94)00334-3.

[19] S.W.H. Eijt, R. Kind, S. Singh, H. Schut, W.J. Legerstee, R.W.A. Hendrikx, V.L. Svetchnikov, R.J. Westerwaal, B. Dam, Positron Depth Profiling of the Structural and Electronic Structure Transformations of Hydrogenated Mg-Based Thin Films. J. Appl. Phys. (2009), 105 (4), 043514. https://doi.org/10.1063/1.3075762.

[20] S.M.T. Beck, W. Anwand, A. Wagner, G. Brauer, A. Beck, A. Ocherashvili, O. Hen, S. Haroush, Y. Eisen, D. Moreno, Investigations of HAVAR® Alloy Using Positrons. Defect Diffus. Forum (2012), 331, 95–112. https://doi.org/10.4028/www.scientific.net/DDF.331.95.

[21] D. Giebel, J. Kansy, LT10 Program for Solving Basic Problems Connected with Defect Detection. Phys. Procedia (2012), 35, 122–127. https://doi.org/10.1016/j.phpro.2012.06.022.

[22] Y. Ortega, J. Río, Study of Mg–Ca Alloys by Positron Annihilation Technique. Scr. Mater. (2005), 52 (3), 181–186. https://doi.org/10.1016/j.scriptamat.2004.09.033.

[23] Y. Cerenius, K. Ståhl, L.A. Svensson, T. Ursby, Å. Oskarsson, J. Albertsson, A. Liljas, The Crystallography Beamline I711 at MAX II. J. Synchrotron Radiat. (2000), 7 (4), 203–208. https://doi.org/10.1107/S0909049500005331.

[24] F.J. Martínez-Casado, M. Ramos-Riesco, J.A. Rodríguez-Cheda, F. Cucinotta, E. Matesanz, I. Miletto, E. Gianotti, L. Marchese, Z. Matěj, Unraveling the Decomposition Process of Lead(II) Acetate: Anhydrous Polymorphs, Hydrates, and Byproducts and Room Temperature Phosphorescence. Inorg. Chem. (2016), 55 (17), 8576–8586. https://doi.org/10.1021/acs.inorgchem.6b01116.

[25] Z. Matěj, R. Kužel, L. Nichtová, XRD Total Pattern Fitting Applied to Study of Microstructure of TiO_2 Films. Powder Diffr. (2010), 25 (2), 125–131. https://doi.org/10.1154/1.3392371.

[26] W. Yang, Z.J. Zhu, J.J. Wang, Y.C. Wu, T. Zhai, G.-L. Song, Slow Positron Beam Study of Corrosion Behavior of AM60B Magnesium Alloy in NaCl Solution. Corros. Sci. (2016), 106, 271–280. https://doi.org/10.1016/j.corsci.2016.02.012.

[27] I. Makkonen, M.J. Puska, Energetics of Positron States Trapped at Vacancies in Solids. Phys. Rev. B (2007), 76 (5), 054119. https://doi.org/10.1103/PhysRevB.76.054119.

[28] O.V. Boev, M.J. Puska, R.M. Nieminen, Electron and Positron Energy Levels in Solids. Phys. Rev. B (1987), 36 (15), 7786–7794. https://doi.org/10.1103/PhysRevB.36.7786.

[29] M.J. Puska, P. Lanki, R.M. Nieminen, Positron Affinities for Elemental Metals. J. Phys. Condens. Matter (1989), 1 (35), 6081–6094. https://doi.org/10.1088/0953-8984/1/35/008.

[30] J. Čížek, I. Prochazka, G. Brauer, W. Anwand, R. Kuzel, M. Cieslar, R.K. Islamgaliev, Ultra Fine Grained Copper Prepared by High Pressure Torsion: Spatial Distribution of Defects from Positron Annihilation Spectroscopy. In Nanomaterials by Severe Plastic Deformation; M. Zehetbauer, R.Z. Valiev, Eds. Wiley-VCH Verlag GmbH & Co. KGaA: Weinheim, FRG, 2005; pp 407–412. https://doi.org/10.1002/3527602461.ch7b.

[31] J. Čížek, I. Procházka, O. Melikhova, G. Brauer, W. Anwand, R. Kužel, M. Cieslar, R.K. Islamgaliev, Investigation of Spatial Distribution of Defects in Ultra-Fine Grained Copper. Appl. Surf. Sci. (2002), 194 (1–4), 140–144. https://doi.org/10.1016/S0169-4332(02)00114-9.

[32] P. Minárik, R. Král, J. Čížek, F. Chmelík, Effect of Different c/a Ratio on the Microstructure and Mechanical Properties in Magnesium Alloys Processed by ECAP. Acta Mater. (2016), 107, 83–95. https://doi.org/10.1016/j.actamat.2015.12.050.

[33] H.-J. Lee, S.K. Lee, K.H. Jung, G.A. Lee, B. Ahn, M. Kawasaki, T.G. Langdon, Evolution in Hardness and Texture of a ZK60A Magnesium Alloy Processed by High-Pressure Torsion. Materials Science and Engineering: A. (2015), 630, 90–98. https://doi.org/10.1016/j.msea.2015.02.011.

[34] L.L. Rokhlin, Magnesium Alloys Containing Rare Earth Metals: Structure and Properties, 0 ed. CRC Press, (2003). https://doi.org/10.1201/9781482265163.

[35] L.C. Smedskjaer, M. Manninen, M.J. Fluss, An Alternative Interpretation of Positron Annihilation in Dislocations. J. Phys. F Met. Phys. (1980), 10 (10), 2237–2249. https://doi.org/10.1088/0305-4608/10/10/019.

[36] H. Häkkinen, S. Mäkinen, M. Manninen, Edge Dislocations in Fcc Metals: Microscopic Calculations of Core Structure and Positron States in Al and Cu. Phys. Rev. B (1990), 41 (18), 12441–12453. https://doi.org/10.1103/PhysRevB.41.12441.

[37] G.M. Hood, Comments on Positron Annihilation and the Vacancy Properties of Mg. Phys. Rev. B (1982), 26 (2), 1036–1037. https://doi.org/10.1103/PhysRevB.26.1036.

[38] A. Seeger, Investigation of Point Defects in Equilibrium Concentrations with Particular Reference to Positron Annihilation Techniques. J. Phys. F Met. Phys. (1973), 3 (2), 248–294. https://doi.org/10.1088/0305-4608/3/2/003.

[39] T.E. Jackman, C.W. Schulte, J.L. Campbell, P.C. Lichtenberger, I.K. Mackenzie, M.R. Wormald, Positron Annihilation Gamma Ray Lineshapes in Metals. J. Phys. F Met. Phys. (1974), 4 (1), L1–L5. https://doi.org/10.1088/0305-4608/4/1/001.

[40] P. Brunner, F. Brumbauer, E.-M. Steyskal, O. Renk, A.-M. Weinberg, H. Schroettner, R. Würschum, Influence of High-Pressure Torsion Deformation on the Corrosion Behaviour of a Bioresorbable Mg-Based Alloy Studied by Positron Annihilation. Biomater. Sci. 2021, 9 (11), 4099–4109. https://doi.org/10.1039/D1BM00166C.

[41] J. Dryzek, Positron Annihilation Studies of Recrystallization in the Subsurface Zone Induced by Friction in Magnesium—Effect of the Inhomogeneity on Measured Positron Annihilation Characteristics. Appl. Phys. A (2014), 114 (2), 465–475. https://doi.org/10.1007/s00339-013-7667-6.

[42] Bulk Nanostructured Materials, 1st ed. M.J. Zehetbauer, Y.T. Zhu, Eds. Wiley, (2009). https://doi.org/10.1002/9783527626892.

[43] J. Čížek, Characterization of Lattice Defects in Metallic Materials by Positron Annihilation Spectroscopy: A Review. J. Mater. Sci. Technol. (2018), 34 (4), 577–598. https://doi.org/10.1016/j.jmst.2017.11.050.

[44] G. Ribárik, J. Gubicza, T. Ungár, Correlation between Strength and Microstructure of Ball-Milled Al–Mg Alloys Determined by X-Ray Diffraction. Mater. Sci. Eng. A (2004), 387–389, 343–347. https://doi.org/10.1016/j.msea.2004.01.089.

[45] R.K. Islamgaliev, F. Chmelik, R. Kuzel, Thermal Stability of Submicron Grained Copper and Nickel. Mater. Sci. Eng. A (1997), 237 (1), 43–51. https://doi.org/10.1016/S0921-5093(97)00107-X.

[46] L. Lutterotti, S. Gialanella, X-ray diffraction characterization of heavily deformed metallic specimens. Acta Mater. (1998), 46 (1), 101–110. https://doi.org/10.1016/S1359-6454(97)00222-X.

[47] P. Scardi, M. Leoni, Whole powder pattern modelling. Acta Cryst. (2002), A58, 190–200. https://doi.org/10.1107/S0108767301021298.

[48] G. Ribárik, B. Jóni, T. Ungár, The Convolutional Multiple Whole Profile (CMWP) Fitting Method, a Global Optimization Procedure for Microstructure Determination. Crystals (2020), 10(7), 623. https://doi.org/10.3390/cryst10070623.

[49] I.C. Dragomir, T. Ungár, Contrast Factors of Dislocations in the Hexagonal Crystal System. J Appl Crystallogr 2002, 35 (5), 556–564. https://doi.org/10.1107/S0021889802009536.

[50] P.S. Roodposhti, A. Sarkar, K.L. Murty, Scattergood, Dislocation Density Evolution During Creep of AZ31 Mg Alloy: A Study by X-Ray Diffraction Line Profile Analysis. Metallogr. Microstruct. Anal. 2015, 4 (5), 337–343. https://doi.org/10.1007/s13632-015-0220-6.

[51] R. Kužel, P. Klimanek, X-Ray Diffraction Line Broadening Due to Dislocations in Non-Cubic Materials. II. The Case of Elastic Anisotropy Applied to Hexagonal Crystals. J Appl Crystallogr 1988, 21 (4), 363–368. https://doi.org/10.1107/S002188988800336X.

[52] R. Kužel, P. Klimanek, X-Ray Diffraction Line Broadening Due to Dislocations in Non-Cubic Crystalline Materials. III. Experimental Results for Plastically Deformed Zirconium. J Appl Crystallogr 1989, 22 (4), 299–307. https://doi.org/10.1107/S0021889889001585.

[53] R.B. Figueiredo, T.G. Langdon, Development of Structural Heterogeneities in a Magnesium Alloy Processed by High-Pressure Torsion. Mater. Sci. Eng. A (2011), 528 (13–14), 4500–4506. https://doi.org/10.1016/j.msea.2011.02.048.

[54] S.A. Alsubaie, Y. Huang, T.G. Langdon, Hardness Evolution of AZ80 Magnesium Alloy Processed by HPT at Different Temperatures. J. Mater. Res. Technol. (2017), 6 (4), 378–384. https://doi.org/10.1016/j.jmrt.2017.05.004.

[55] A.Y. Khereddine, F.H. Larbi, M. Kawasaki, T. Baudin, D. Bradai, T.G. Langdon, An Examination of Microstructural Evolution in a Cu–Ni–Si Alloy Processed by HPT and ECAP. Mater. Sci. Eng. A (2013), 576, 149–155. https://doi.org/10.1016/j.msea.2013.04.004.

[56] J. Čížek, I. Procházka, B. Smola, I. Stulíková, R. Kužel, Z. Matěj, V. Cherkaska, R. K. Islamgaliev, O. Kulyasova, Defects in Ultra-Fine Grained Mg and Mg-Based Alloys Prepared by High Pressure Torsion Studied by Positron Annihilation. Acta Phys. Pol. A (2005), 107 (5), 738–744. https://doi.org/10.12693/APhysPolA.107.738.

[57] W.T. Sun, X.G. Qiao, M.Y. Zheng, Y. He, N. Hu, C. Xu, N. Gao, M. J. Starink, Exceptional Grain Refinement in a Mg Alloy during High Pressure Torsion Due to Rare Earth Containing Nanosized Precipitates. Mater. Sci. Eng. A (2018), 728, 115–123. https://doi.org/10.1016/j.msea.2018.05.021.